

# Landslide Vulnerability Identification Based on the Geological Condition, GIS Calculation, and Field Validation in the Tropical Area

Kausarian, Husnul

Engineering Geological Program, Faculty of Engineering, Universitas Islam Riau

Septio, Ghenady

Engineering Geological Program, Faculty of Engineering, Universitas Islam Riau

Josaphat Tetuko Sri Sumantyo

Center for Environmental Remote Sensing, Chiba University

Tutuko, Pindo

Department of Architecture, University of Merdeka Malang

他

<https://doi.org/10.5109/7161458>

---

出版情報 : Evergreen. 10 (4), pp.2423-2438, 2023-12. 九州大学グリーンテクノロジー研究教育センター

バージョン :

権利関係 : Creative Commons Attribution 4.0 International

# Landslide Vulnerability Identification Based on the Geological Condition, GIS Calculation, and Field Validation in the Tropical Area

Husnul Kausarian<sup>1\*</sup>, Ghenady Septio<sup>1,2</sup>, Josaphat Tetuko Sri Sumantyo<sup>3</sup>, Pindo Tutuko<sup>4</sup>, Adi Suryadi<sup>1</sup> and Fitri Mairizki<sup>1</sup>

<sup>1</sup>Engineering Geological Program, Faculty of Engineering, Universitas Islam Riau, Indonesia

<sup>2</sup>Engineering Geological Program, Faculty of Engineering, Universitas Gadjah Mada, Indonesia

<sup>3</sup>Center for Environmental Remote Sensing, Chiba University, Japan

<sup>4</sup>Department of Architecture, University of Merdeka Malang

\*Author to whom correspondence should be addressed:

Email: husnulkausarian@eng.uir.ac.id

(Received September 19, 2023; Revised October 30, 2023; accepted October 30, 2023).

**Abstract:** This study focuses on mapping areas that are vulnerable to landslides in tropical areas by taking a case study in the district of XIII Koto Kampar, Riau Province, Indonesia, which is in the tropical areas on 0°01'40"N to 0°27'00"N and 100°28'30"E – 101°14'30"E. This study aims to determine the characteristics of landslide assessment and the zone mapping of the landslide vulnerability level using a comprehensive method from primary and secondary data. Primary data are Geological Data, Digital Elevation Model (DEM), and Landsat-8 OLI Satellite Imagery Data. Furthermore, secondary data consists of Lithological Data, Slopes Data, Relative Relief Data, Land Wetness Data, Land Cover Data, and 2021 Rainfall Data. The analysis of landslide vulnerability areas in this study is processed using a Geographic Information System (GIS) for scoring and classifying landslide vulnerability areas. From all the processed data, an analysis is carried out to connect and overlay them to get complete data in determining the zoning of the landslide vulnerability classification in the research area. The study in this research area resulted in a landslide vulnerability score and classification that was divided into 4 categories: Very Low Vulnerability area (22.6%), Low Vulnerability area (61.8%), Medium Vulnerability area (15.2%), High Vulnerability area (0.4%).

Keywords: Landslide Vulnerability, Geological Information, GIS, Landsat-8 OLI, Tropical Area

## 1. Introduction

The landslide vulnerability of an area can be seen from how often landslides occur and can also be seen from the geological condition of the area<sup>1-5</sup>. A landslide is a movement of soil mass on the slope plane, from high elevation to low elevation at a time<sup>6-9</sup>. The trigger for this movement of soil mass is internal instability in the soil, where the shear strength of the soil has been exceeded. The triggers are various, such as earthquakes, heavy rains that saturate the soil to increase the pore water pressure of the soil, and others<sup>10-12</sup>. One form to minimize the occurrence of landslides can be done by mapping the source area of the landslide disaster so that it can map the area that is likely to be affected by the landslide disaster and make mitigation actions in the event of a landslide<sup>13-18</sup>.

Identification, analysis, and mapping of landslide vulnerability in tropical areas are carried out to gain

knowledge of areas that are very vulnerable to landslides and can adjust the conditions of the case study area by processing regional lithological or geological maps, slope maps, relative relief map, land cover map, land wetness, and rainfall data by knowing the characteristics and mapping the level of vulnerability zoning.

The District of XIII Koto Kampar, Regency of Kampar, Province of Riau, Indonesia; an area of 927.17 km<sup>2</sup> which is located between 0°01'40"N to 0°27'00"N and 100°28'30"E– 101°14'30"E (Fig. 1) was chosen as the appropriate area for this research because it describes a suitable situation related to the potential for landslides in tropical areas.

## 2. Geological and Research Background

Geologically, Kampar Regency is in the Central Sumatra Basin, part of the back-arc basin<sup>19</sup>. Back-arc basins develop along the western and southern coasts of

the Sunda Shelf<sup>20,21)</sup> (Fig. 2). Rocks in the Pre-Tertiary Period underwent an extensional process, causing the formation of a structure in the form of a half-graben which experienced an uplift of tertiary age.

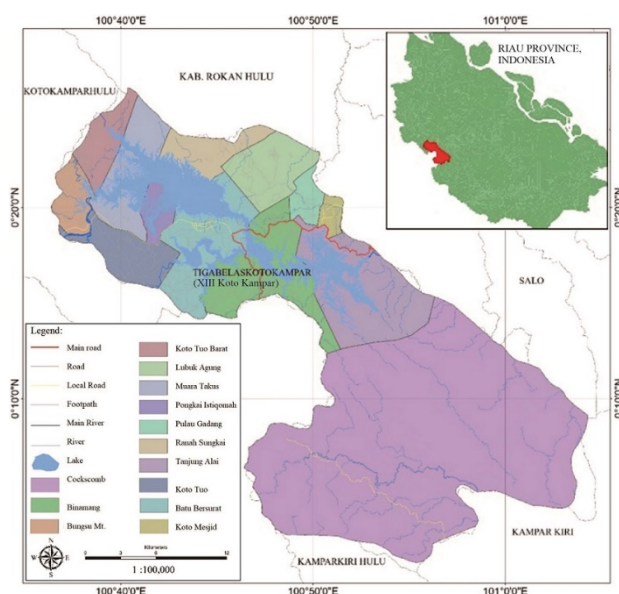


**Fig. 1:** Location of the District of XIII Koto Kampar.

Then there is the erosion process of the rock that has undergone an uplift. The erosion process results will be carried away and settle around the river flow and produce Alluvial deposits<sup>22)</sup>. This research's objective is to the location in District XIII Koto Kampar, which has a landslide vulnerability. Mapping the vulnerability of this landslide area is to classify each landslide vulnerability area from the lowest to the highest by dividing the area based on the factors that cause landslides.

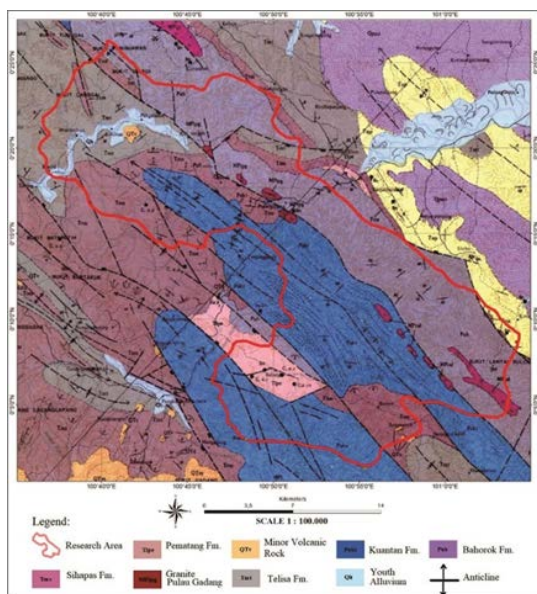


**Fig. 2:** Regional Geological Map of the District of XIII Koto Kampar (Modified from Geological Map of Pekanbaru Sheet, Clarke et al., 1982).

The research in this area aims to find out which rocks have high and low weather abilities by using the groundwater center and the geological environment of the Ministry of Energy and Mineral Resources, the Republic of Indonesia, as an initial reference. After the data was processed, the data was corrected using the 2004 Pekanbaru Bakosurtanal Map<sup>23)</sup> to ensure that each lithology in the area was the same as the existing formations in the study area.

In the lithological analysis, several lithologies were obtained with scores that have been classified and from the results obtained from the field (Fig. 3), there are slate, phyllite, and schist lithology, which has an area of  $\pm 340.41 \text{ km}^2$  with an area percentage of 35 % and the lithology of Wake, Conglomerate and Turbidite wake rocks has an area of  $\pm 323.39 \text{ km}^2$  with an area percentage of 33%. The relationship between lithological data and landslides in the study area can be identified with the existing lithology in the XIII Koto Kampar area, which is dominated by sedimentary lithology in the form of conglomerates, sandstones, breccias which influence slope stability where these sedimentary rocks have properties that are not solitary and easily eroded. Besides sedimentary rocks, the study area is also dominated by metamorphic rocks, namely slate, phyllite, and schist. Metamorphic rock has more detached properties than sedimentary rocks, and when compared to igneous rock, which is more compact, hard, and still tends to have a low vulnerability to landslides. These results were then validated by direct observation in the field.



**Fig. 3:** The lithology found in the District of XIII Koto Kampar: a). Alluvium, b). Metamorphic Rock from Kuantan Formation, c). Conglomerate from Sihapas Formation, d). Coarse grain Sandstone from Sihapas Formation, e). Sandstone from Sihapas Formation, f). Wacke conglomerate from Bahorok Formation, g). Wacke turbidite from Bahorok Formation.

The relationship between lithological and landslides in this research area can be identified with the lithology of sedimentary and metamorphic rocks. The sediments in this research area consist of conglomerates, sandstones, and breccias influencing slope stability. This type of sedimentary rock has properties that are not solid and

easily eroded. In addition, the metamorphic rocks in this research area are dominated by slate, phyllite, and schist. Metamorphic rock lithology has more solid properties than sedimentary rocks, and when compared to igneous rocks, igneous rocks are more compact, hard, and have a low vulnerability to landslides. Because the lithological content in this area consists of sedimentary and metamorphic rocks that have begun to weather, the potential for landslide vulnerability in this research area is more significant.

### 3. Methodology

The research method is carried out by determining the zoning by giving a weighting score. Furthermore, the geographical information system (GIS) method is used to classify the factors causing landslides<sup>24-30</sup> and classify the landslide vulnerability zone<sup>31-37</sup>. The factors used to classify the area's vulnerability to landslides are slope, lithology, land wetness, relative relief, land cover, and rainfall as supporting data in the study. The method can then be translated into a numerical classification scheme called the landslide hazard evaluation factor (LHEF)<sup>38-42</sup>.

The data used in this study are primary data and secondary data. Primary data consists of 1. Geological mapping, 2. Field validation, 3. Landsat-8 OLI satellite image data, 4. Digital Elevation Model, 5. Soil and rock samples analysis, 6. GIS data processing using relevant software. At the same time, the secondary data used include 1. Data on Regional Spatial Planning for the Kampar Regency area obtained from Kampar Government; 2. Lithological Data (shapefile format / SHP) of Riau Province from the Centre for Groundwater and Geology Environmental Management of the Ministry of Energy and Mineral Resources of the Republic of Indonesia; 3. Slope Data obtained from the Digital Elevation Model (DEM) of Alaska Satellite Facility 2020; 4. Relative Relief Data obtained from the Digital Elevation Model (DEM) of Alaska Satellite Facility 2020; 5. Land Cover Data obtained from Landsat-8 OLI United States Geological Survey (USGS) imagery; 6. Land Wetness Data was obtained using Landsat-8 OLI United States Geological Survey (USGS) image; 7. The straightness data of the slope direction is obtained from the Digital Elevation Model (DEM) Alaska Satellite Facility 2020; 8. Rainfall data were obtained from the Board of Meteorology, Climatology, and Geophysics of the Republic of Indonesia.

This research uses a numerical grading scheme called the landslide hazard evaluation factor (LHEF). LHEF is a numerical grading system on the main factors causing landslides. These factors include lithology, slope, relative relief, land cover, and groundwater conditions. The maximum value for the sum of all the values of these factors is ten values that have the greatest vulnerability. Furthermore, to determine these factors, corrections are made to the satellite imagery used, namely radiometric corrections and geometry corrections. Where in general,

radiometric correction can be derived in the following formula:

$$L\lambda = MLQ_{cal} + AL \dots\dots\dots(1)$$

Where:

$L\lambda$  is TOA spectral radiance (Watts/(m \* srad \*  $\mu$ m))

$ML$  is Rescaling factor value that can be obtained from metadata image ( $RADIANCE\_MULT\_BAND\_x$ , where  $x$  is the band number)

$AL$  is The rescaling factor value of the band, which can be obtained from the metadata image ( $RADIANCE\_ADD\_BAND\_x$ , where  $x$  is the band number)

$Q_{cal}$  is The band to be a radiometric correction (DN)

After the radiometric correction is made, it is necessary to carry out geometric correction. In the radiometric correction process, the error rate (RMSE) must be below one (<1) with consideration of adjustments from the point of the earth's location, where the smaller the RMSE value, the better the level of accuracy. The general equation for geometric correction is as follows:

$$\text{minimum total GCP} = (t + 1)(t + 2)/2 \dots\dots\dots(2)$$

Where:

$GCP$  is Ground Control Point

$t$  is order

Furthermore, lithological analysis was carried out to determine the lithological conditions. The type of lithology is very influential on the possibility of a slope for landslides.

The following method is slope analysis, where the slope is the angle formed between the ground surface plane and the normal plane. The history of geomorphological processes influences the size of the slope in an area. The slope map is made from a topographic map divided based on the number of contour lines that pass through one slope. The slope in this method is classified into five classes, namely very steep (>45°), steep (25°-35°), moderate (25°-35°), flat (16°-25°), and very flat (≤15°). The higher the slope angle, the greater value of landslide vulnerability.

Furthermore, the relative relief analysis is carried out. Relative Relief is a quantity that shows the difference in elevation between the highest peak and the lowest valley on an individual facet. The relative relief in this method is classified into three classes, namely low (<100 m), medium (100-300 m), and high (> 300 m). The greater the relative relief value, the greater the value of landslide susceptibility.

The following method is land cover analysis. Land cover is an indirect indication of slope stability. Barren land and sparsely planted land will quickly erode, causing unstable slopes. On the other hand, land planted with many plants will be more resistant to erosion, so the slope is more stable. It is done by supervised classification in identifying images to create the land cover. This

classification is fixed on pixels into classes determined by the method used in the category used. The guided classification analysis first needs to determine several training sample areas in the land cover area to be trained. Areas with the same pixel value will be classified as the same category. Areas that have a high score will be more vulnerable to landslides.

After the land cover analysis, it continued to the Land Wetness Analysis. This analysis is expected to represent the condition of the groundwater. The surface water conditions in this method are classified into five classifications: dry, moist, wet, soaked and flowing. In the stage of making the map, Wetness is carried out using the Normalized Difference Water Index (NDWI) method. This method is used to determine the wetness in satellite imagery. In this method, the green band (band 3) is used to optimize the reflection of water bodies and uses the near-infrared band (band 5). Band 5 is used to minimise the reflection of water bodies. If the NDWI value is greater than zero, it is assumed to represent the surface of the water body, and if the value is less than or the same, it is a non-water surface. Areas that have a high wetness value will be more vulnerable to landslides. NDWI is formulated as follows:

$$NDWI = \frac{Band\ 3\ (green) - Band\ 5\ (NIR)}{(Band\ 3\ (green) + Band\ 5\ (NIR))} \dots \dots \dots (3)$$

Where:

*Band 3* is To determine the sensitivity of the peak of the reflection of vegetation.

*Band 5* is To determine biomass content, vegetation type, and coastline type.

The following method is the straightness analysis of the slope, which is carried out by observing the lineament pattern from the combined DEM data and Landsat-8 OLI imagery. This lineament can be interpreted as the same element as geomorphology that describes the geological structure or relationship with lithology. The straightness on the earth's surface is reflected by the morphological straightness caused by the relief, such as the straightness of valleys, mountains, and rivers where this straight line is seen from its location facing the sun, the more exposed to sunlight, the greater the potential for weathering, which can cause landslides.

The subsequent analysis is the rainfall data analysis. This analysis is very influential on landslides. To find out how the state of influence is, rainfall data is taken from the Board of Meteorology, Climatology, and Geophysics of the Republic of Indonesia to get an average monthly value in one year covering the entire research area so that it can be seen its effect on vulnerability to landslides. The rainfall data were taken from January to December 2021.

The following analysis is the calculated Total Estimated Hazard (TEHD) and landslide hazard zoning. This analysis is an index of the probability of a scoring part to determine the landslide vulnerability area. The value of

the total hazard of landslide hazard is the sum of the hazard values of lithology, slope, relative relief, land cover, and groundwater conditions. After the estimated value of the vulnerability hazard is obtained, the level of vulnerability to landslides can be identified. A large score value has a significant vulnerability, while a small value has a low vulnerability.

After the data is obtained, the next step is to conduct the analysis and calculations needed for landslide analysis. The first step is to assign a scoring/weighting to the map according to the parameters and criteria. Next, an overlay process is carried out by overlaying calculated parameter maps (slope map, relative relief map, lithology map, land cover map, and land wetness map). The determination of landslide vulnerability areas using GIS can be seen in Figure 4. The analysis results will later produce the value of the TEHD range. Furthermore, this value is converted at several levels of landslide hazard. After getting all the data, a complete analysis is carried out using several software such as Google Earth, ArcMap, and ArcScene. All the software is used to produce thematic maps, such as slope maps, relative relief maps, lithological maps, land cover maps, and land wetness maps which are then overlaid and produce landslide hazard maps.

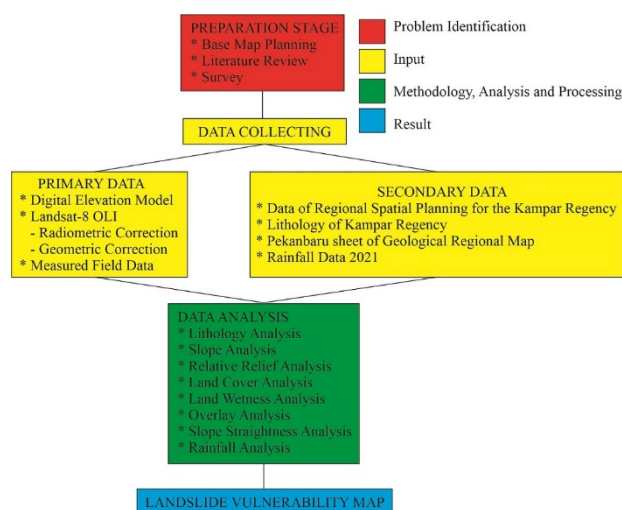


**Fig. 4:** Flowchart of the Research Conducted for the Landslide Vulnerability Map in the District of XIII Koto Kampar.

## 4. Result And Discussion

### 4.1 Image Correction

Image correction was carried out to model and classify land cover and wetness in this research area as the main input to produce the map and the analysis. The image data used is in the form of Landsat-8 OLI imagery data in 2021, which was obtained from the United States Geological Survey (USGS). Corrections were made in the form of radiometric correction and geometry correction.

#### 4.1.1 Radiometric Correction

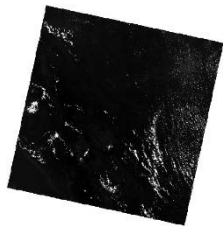
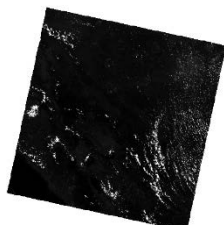
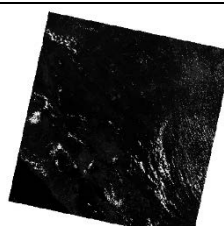
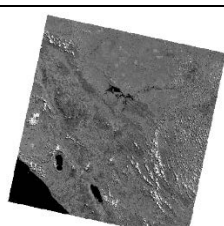
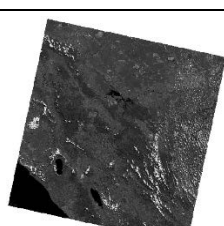
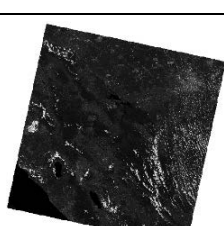
The radiometric correction was carried out in the 2021



Landsat-8 OLI image obtained from USGS (Table 1). In this image, the correction was carried out on each Band, from Band 2 to Band 7, which was carried out in 2 stages,

namely, at-sensor radiant and Top of the Atmosphere (TOA).

Table 1. Landsat-8 OLI Radiometry Correction for each band used in the District of XIII Koto Kampar.

Band	Original Image	At-Sensor Radiant	Top of the Atmosphere (TOA)	Corrected Image
2	46628	576,362	0,715846	
3	46707	574,384	0,778962	
4	49281	546,586	0,875365	
5	54721	360,836	0,952445	
6	40157	89,7366	0,940303	
7	38449	30,246	0,974015	

From this table, each pixel is in each band and has a different value. It can also be seen from the table that the correction difference for each band is processed through

radiometric correction from the at-radiant sensor to the Top of the Atmosphere (TOA) stage. In this correction, it can be stated that a large pixel value indicates a

disturbance in the atmosphere, which causes the object's reflection value not to be the original value. The results of this radiometric correction were used to analyse land cover and land wetness in the XIII Koto Kampar area, Kampar Regency, Riau Province, Indonesia, as the research area.

After getting the original value from the radiometric correction, merging each band into one image, commonly called a multispectral composite band, is carried out. The purpose of merging this image is to make combining each band in the image easier. Fig. 5 shows the composite band after the correction.

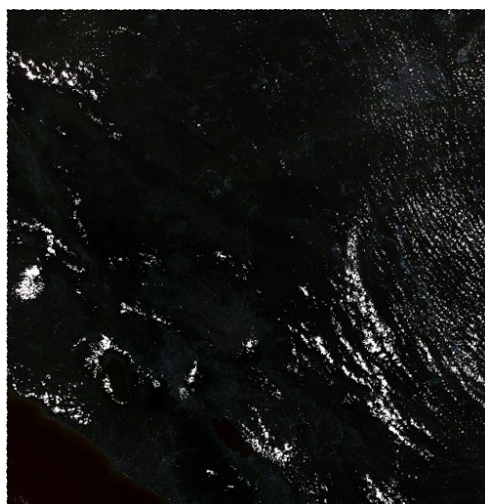


Fig. 5: Multispectral composite band of the District of XIII Koto Kampar.

#### 4.1.2 Geometric Correction

Geometry Correction is performed to place the image in its actual position. Geometry correction was carried out on the Landsat-8 OLI image, which refers to the geospatial data on the Indonesia Geomorphological map in the XIII Koto Kampar District Riau province, Indonesia. Geometry correction was carried out using Ground Control Point and performed at 4 points on the Landsat-8 OLI image in the research area (Fig. 6).

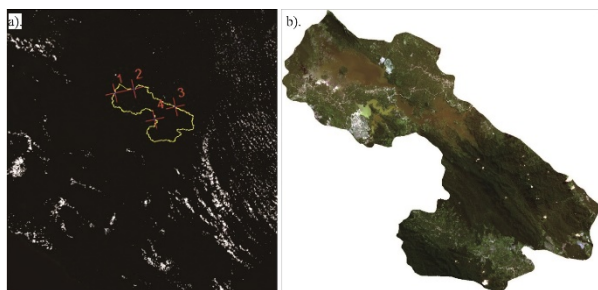


Fig. 6: a). Geometry Correction on Landsat-8 OLI image in the District of XIII Koto Kampar, b). Cropping Research Area (the District of XIII Koto Kampar) from Landsat-8 OLI image.

In the Geometry Correction, the Root Square Mean Error (RSME) must be below  $<0.5$  by adjusting the actual point of the earth's position. The smaller of RSME value, the better of accuracy level. Table 2 shows that the RSME value is below  $<0.5$ . It shows that the research area geometrically corrected image is feasible for this study.

Table 2. Root Square Mean Error (RSME) of the Landsat-8 OLI in the District of XIII Koto Kampar.

Coordinate		RMSE
X	Y	
681801,001	43170,040	0,0708646
695145,611	43502,210	
720219,013	25139,771	
704805,687	20266,408	

The following process on this Landsat-8 OLI image is cutting or cropping the area included for the research area. This cropping process is carried out to make it easier to identify and analyse the research area (see Fig. 6).

#### 4.2 Lithological Analysis

Lithological data processing is carried out using vector data in the form of data processed from groundwater and geological environmental data based on the research area. This lithological data is used to determine the lithological description of rocks in the research area to determine which rocks have high and low weathering. Furthermore, it is adjusted to the existing formations in the research area based on the results of field validation.

In the lithology analysis, several lithologies were obtained with scores that have been classified. The results consisted in the lithology analysis with the widest area consisting of Slate, Phyllite, and Schist lithology, which has an area of  $\pm 340.41 \text{ km}^2$  with a percentage of 35%, and the lithology of Wacke, Conglomerate and Turbidite Wacke lithology has an area of  $\pm 323.39 \text{ km}^2$  with a percentage of 33%. The following are the results of the lithological analysis carried out in the research area (Table 3).

The relationship between lithological data and landslides in the research area can be identified as having an influence on slope stability where these sedimentary rocks have properties that are not solid and easily eroded, and the lithological domination followed by metamorphic rocks which are slate, phyllite, and schist. In lithology, metamorphic rocks have more solid properties than sedimentary rocks, and when compared to igneous rocks, which are more compact, hard, and still tend to have a low vulnerability to landslides. After lithological analysis and validation in the field, a geological map can be produced in the research area (Fig. 7).

Table 3. Lithological Distribution in the District of XIII Koto Kampar.

Lithology	Formation (symbol)	Scoring	Total Area (Km <sup>2</sup> )	Percentage (%)
Mudstone, Conglomerate, Breccia, and Conglomerate-sandstone	Pematang (Tipe)	1,3	35,187	3,59%
Acidic Igneous Rock, mainly Granite	Pulau Gadang (MPigt, MPipg, MPiul, MPi)	0,3	18,574	1,90%
Slate, Phyllite, and Schist	Kuantan (Puku)	1,2	340,412	34,73%
Conglomerate, Sandstone, Breccia	Sihapas (Tms)	1.3	168,448	17,19%
grey mud-Limestone, thin Limestone, calcareous Siltstone, and a small amount of glauconite Sandstone	Telisa (Tmt)	0,2	67,154	6,85%
Shale, Siltstone, Mudstone	Tuhur (Mtt)	1,8	1,864	0,19%
Uneroded minor Volcanic rock	Minor volcanic rock (QTv)	0,3	2,465	0,25%
Old Alluvium Consists Of Gravel, Sand, Clay, And Peat	Alluvium (Qp)	1,4	22,391	2,28%
Wacke, wacke Conglomerate and Turbidite	Bahorok (Pub)	1,3	323,392	33,00%

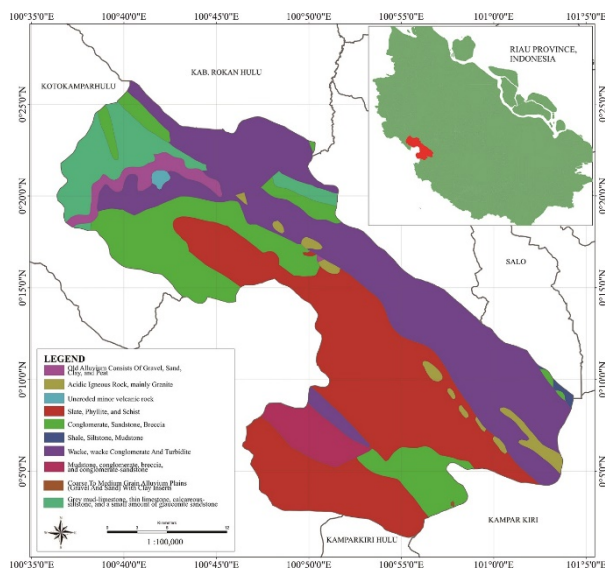


Fig. 7: a). Geological Map of the District of XIII Koto Kampar showing the Lithologies Distribution.

### 4.3 Slope Analysis

Slope analysis found that the area has different types of slope steepness. There are five categories used in this slope. Slope data is used to make or analyse the slope value using digital elevation model (DEM) data. Slope measurement is carried out by the degree of the slope, measured between the height of the slope and the length of the slope used. The relationship between Slope and landslides vulnerability is influenced by the presence of areas with very high steepness. From the calculation, 38% of the area is flat and dominated by water, and the very steep slope is 15% of the total area and consists of rock with weathered conditions. The detailed classification can be seen in Table 4, which shows the slope degree, total area, and percentage of the slope distribution in this research area.

Many rock quarries in this area erode or take part of the

slope, which causes this slope to become unstable. Also, a steep slope makes it more vulnerable to landslide potential. This data is proved from the field validation related to the slope steepness (Fig. 8). After completing all these analysis, the slope map can be produced in this research area (Fig. 9).

Table 4. Classification of Slope Analysis in the District of XIII Koto Kampar.

Slope (°)	Classification	Total Area (Km <sup>2</sup> )	Percentage (%)
< 15	Flat	378,894	38%
16 - 25	Slight Flat	202,492	21%
26 - 35	Slight Steep	147,741	15%
36 - 45	Steep	102,745	11%
> 45	Very Steep	146,494	15%

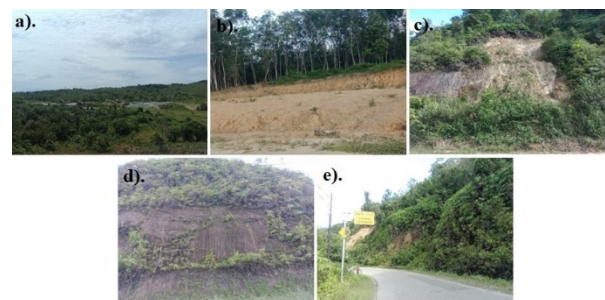


Fig. 8: a). Validation of Slope condition in the field: a). Flat Slope, b). Slight Flat Slope, c). Slight Steep Slope, d). Steep Slope, e). Very Steep Slope.



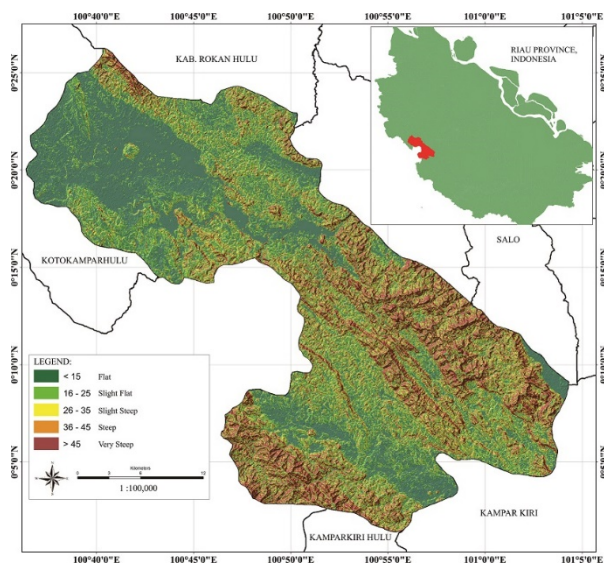


Fig. 9: a). Slope Steepness Distribution of the District of XIII Koto Kampar from the Slope Analysis.

#### 4.4 Relative Relief Analysis

The Relative Relief analysis has three parameters by calculating the standard elevation or a predetermined height (Table 5). Digital elevation model (DEM) data was used to perform a relative relief analysis by mosaics on the DEM data and cropping on the research area (Fig. 10).

The relationship of Relative Relief to landslides is influenced by elevation, where high elevations have a higher landslide vulnerability. In this research area, the lowest elevation starts with a height of about 52 meters above sea level, and the highest elevation area is around 684 meters. The research area is dominated by a low elevation of about 64%, which makes this area a safe condition with very low to low vulnerability to landslides. And at a high elevation of about 11%, this area is highly vulnerable to landslides. This data is validated by field calculation for relative relief (Fig. 11). After all these analyses have been completed, a map of the relative relief in the research area can be generated, as shown in Fig. 12.

Table 5. Classification of the Elevation on the District of XIII Koto Kampar Based on the DEM Analysis.

Elevation (mdpl)	Classification	Total Area (Km <sup>2</sup> )	Percentage (%)
<100	Low	628.044	64%
100 – 300	Moderate	240.214	24%
>300	High	112.242	11%



Fig. 10: Digital Elevation Model (DEM) Data on the District of XIII Koto Kampar.

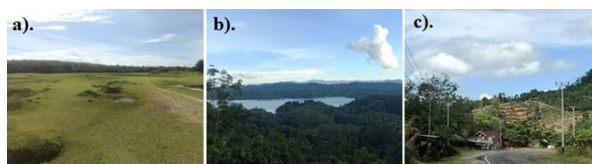


Fig. 11: Field Validation of Relative Relief in the District of XIII Koto Kampar: a). Low Relative Relief, b). Moderate Relative Relief, c). High Relative Relief.

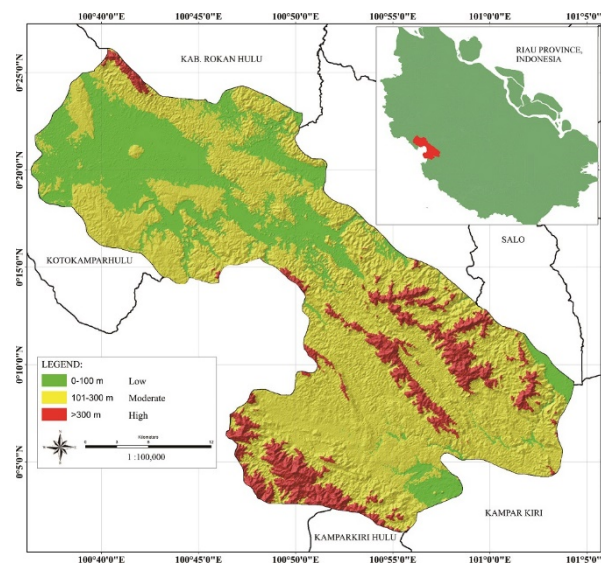


Fig. 12: Relative Relief Map of the District of XIII Koto Kampar.

#### 4.5 Land Cover Analysis

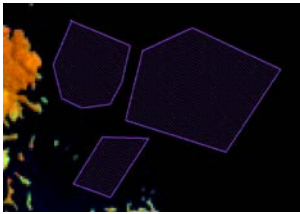
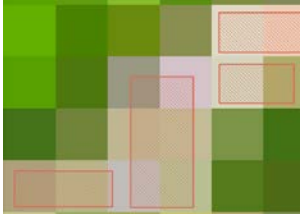
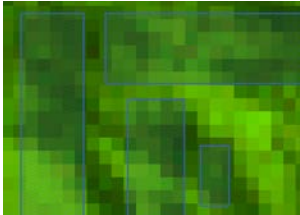
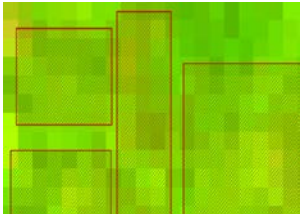
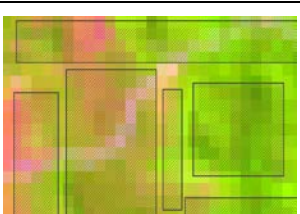
In the land cover analysis, the radiometric and geometric correction process has been completed with a composite band to identify the land cover from Landsat-8 OLI imagery. The land cover analysis uses a classification consisting of 6 parameters, namely water bodies, population areas, dense forest areas, slightly covered by plant areas, rarely covered by plant areas, and open areas used to classify each area to produce land cover maps in this research area.

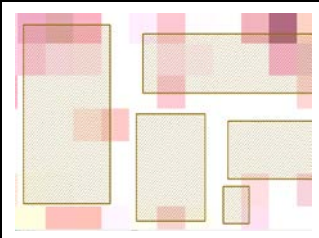
This classification process is carried out by conducting a Training Sample Area in the research area. The more samples are taken, the more precise of accuracy level. The following table shows the results of the training sample carried out on the Landsat-8 OLI imagery in the research area combined in each band (Table 6).

The relationship between land cover and landslides is carried out by the condition of areas with non-vegetated or open areas that are more vulnerable to landslides than areas with dense vegetation. Landslides can also be influenced by land use changes that do not follow the area's geological conditions. In this analysis, the dominant area is covered by dense forest, 38% making this area have

strong stability against soil movement, which makes has a very low to moderate landslide vulnerability. Areas that are rarely covered by plants and open areas significantly affect landslides. Where the results of the analysis carried out on land cover areas in this research area are rarely covered by plants, have an area of 9%, and the open area has about 6%, which causes this area to have moderate to high landslides vulnerability. This data is completed by the field validation related to land cover calculation (Fig. 13). After all these analyses have been conducted, a map of land cover in the research area can be generated (Fig. 14).

Table 6. Training Sample Area Using Band Combination of Landsat-8 OLI in the District of XIII Koto Kampar.

Land Cover	Training Sample Area	Band Combination	Total Area (Km <sup>2</sup> )	Percentage (%)	Description
Water Body (River/ Lake) Area		5-6-4	78,839	8	The dark and blue color indicates a shallow area.
Population Area		7-6-4	14,589	1	The color of each pixel is very striking from the others.
Dense Forest Area		6-5-4	372,640	38	Have a darker shade of green.
Slightly Covered by Plants Area		6-5-4	366,895	37	Bright green color indicating not too dense with vegetation.
Rarely Covered by Plants Area		6-5-4	89,862	9	Green mixed with pink color.

Open Area		7-5-3	57,112	6	Different color (pink) to another.
-----------	---	-------	--------	---	------------------------------------

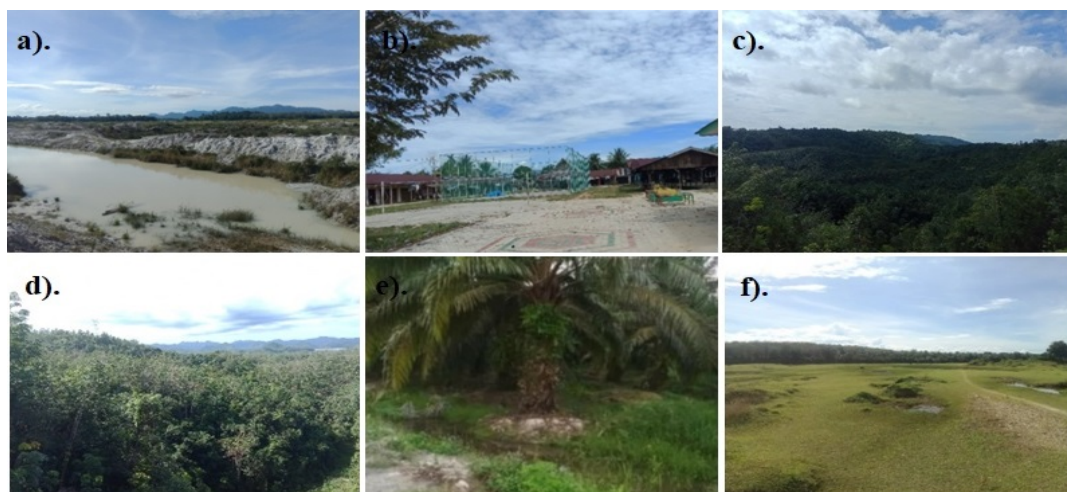


**Fig. 13:** Validation of land cover in the District of XIII Koto Kampar: a). Water Body (River/Lake) Area, b). Population Area, c). Dense Forest Area, d). Slightly Covered by Plants Area, e). Rarely Covered by Plants Area, f). Open Area.

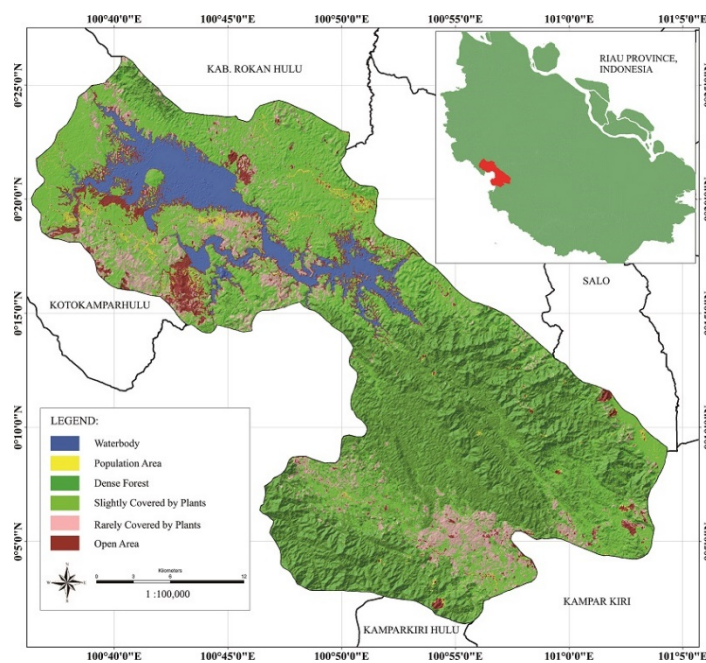


**Fig. 14:** Land Cover Map of the District of XIII Koto Kampar.

#### 4.6 Land Wetness Analysis

Land Wetness analysis is carried out using image identification using Landsat-8 OLI Imagery which has already been carried out with an image correction process in the form of radiometric and geometric correction. Wetness classification analysis consists of 5 classifications (Table 7) carried out using the Normalized Difference Water Index (NDWI) method, which uses

bands 3 and 5, which have been cropped in the research area.

Table 7. Result of Land Wetness Analysis on the District of XIII Koto Kampar.

Land Wetness Classification	Total Area (km <sup>2</sup> )	Percentage (%)
Dry	208,601	21,29%



Moist	374,655	38,23%
Soak	242,720	24,77%
Wet	57,292	5,85%
Flow	96,612	9,86%

The relationship of Land Wetness to landslides is where areas that tend to flow have a greater vulnerability than dry areas. The flowing area is 9.86% of the coverage area in the research area, which has a high landslide vulnerability. The area that has dominated the research area is the moist area, with 38.23% of the total area. Flowing areas have more vulnerability because it can make the rocks in the area weathered and eroded. The wetness of the land is one of the factors that significantly affect the occurrence of landslides, especially in this research area which has a wide of moist and wet areas and areas with slightly steep slopes. This data is completed by

the field validation related to the land wetness (Fig. 15) calculation. After all these analyses have been conducted, a map of the land wetness in the research area can be generated (Fig. 16).

#### 4.7 Straightness of Slope Direction Analysis

Analysis of the direction of the slope is used to show the direction of the slope, which also influences the magnitude of the landslide. The direction of the slope can affect weathering, where the direction of the slope will affect the amount of each sun irradiation. The slope value is instrumental in representing the direction of the slope relative to the direction of sunlight. In this research area, the dominant slope direction is in the southeast, with an area of about 145.354 km<sup>2</sup> and 14.84%. The direction of this slope is shown in the Rose Diagram graphic (Fig. 17). After all the analysis and field validation, a map of the Slope Direction can be generated (Fig. 18).

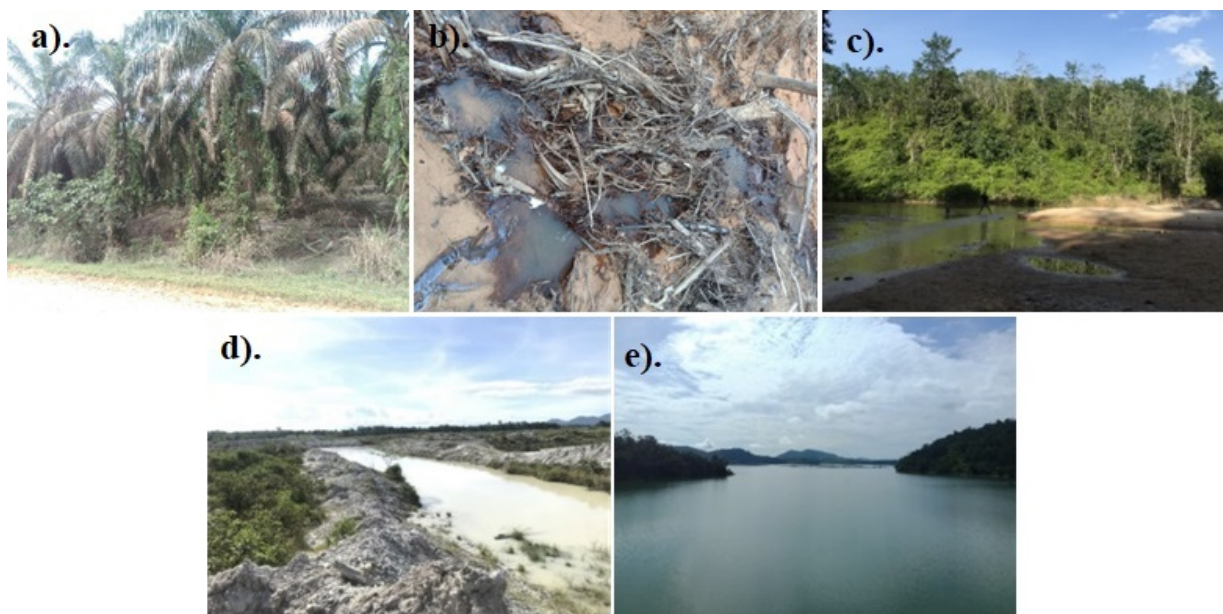


**Fig. 15:** Validation of land wetness in the field: a). Dry Area, b). Moist Area, c). Soak Area, d). Wet Area, e). Flow Area.

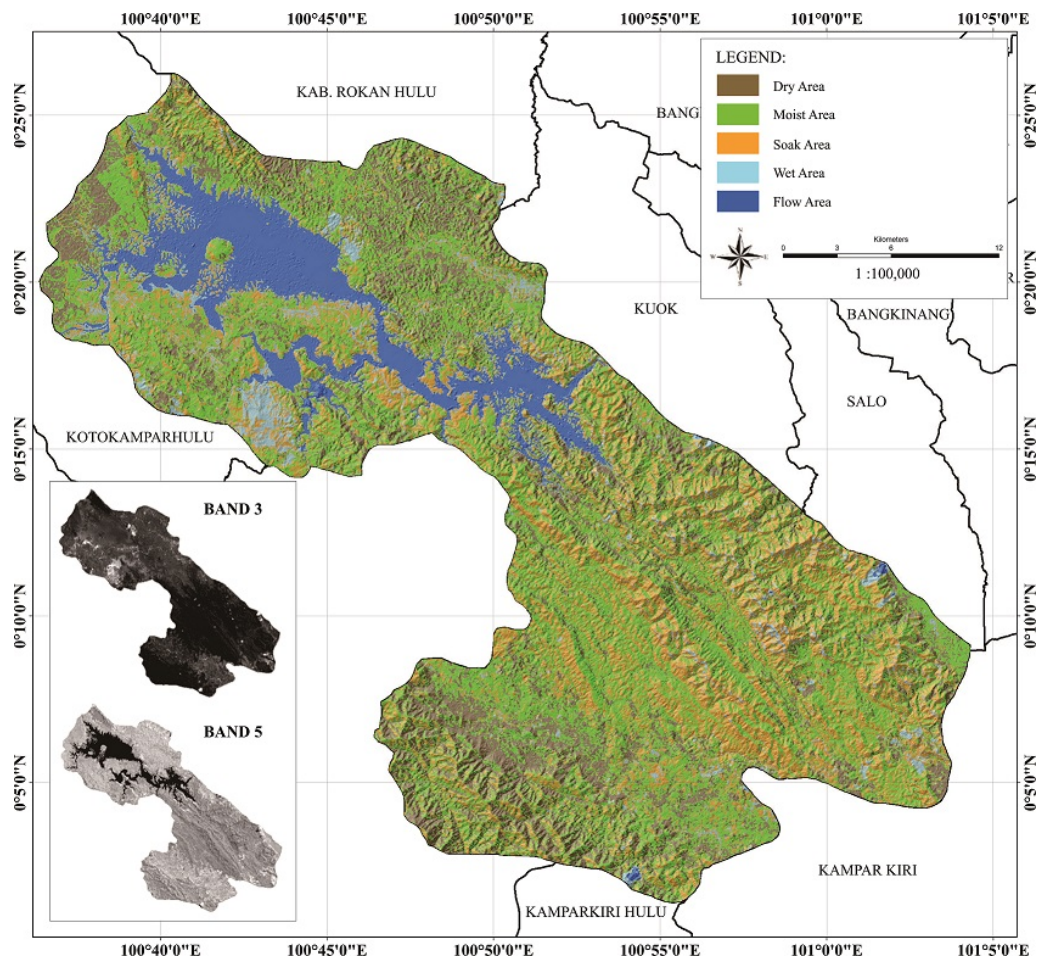


Fig. 16: Land Wetness Map of the District of XIII Koto Kampar.

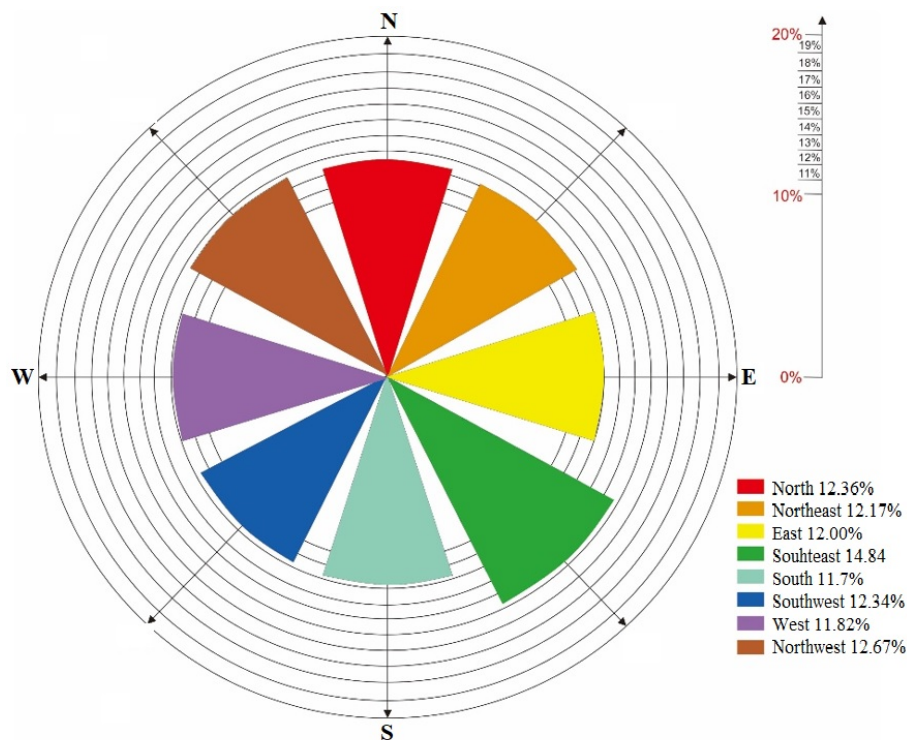


Fig. 17: Rose Diagram of Straightness of the Slope Direction Analysis Calculation in the District of XIII Koto Kampar.



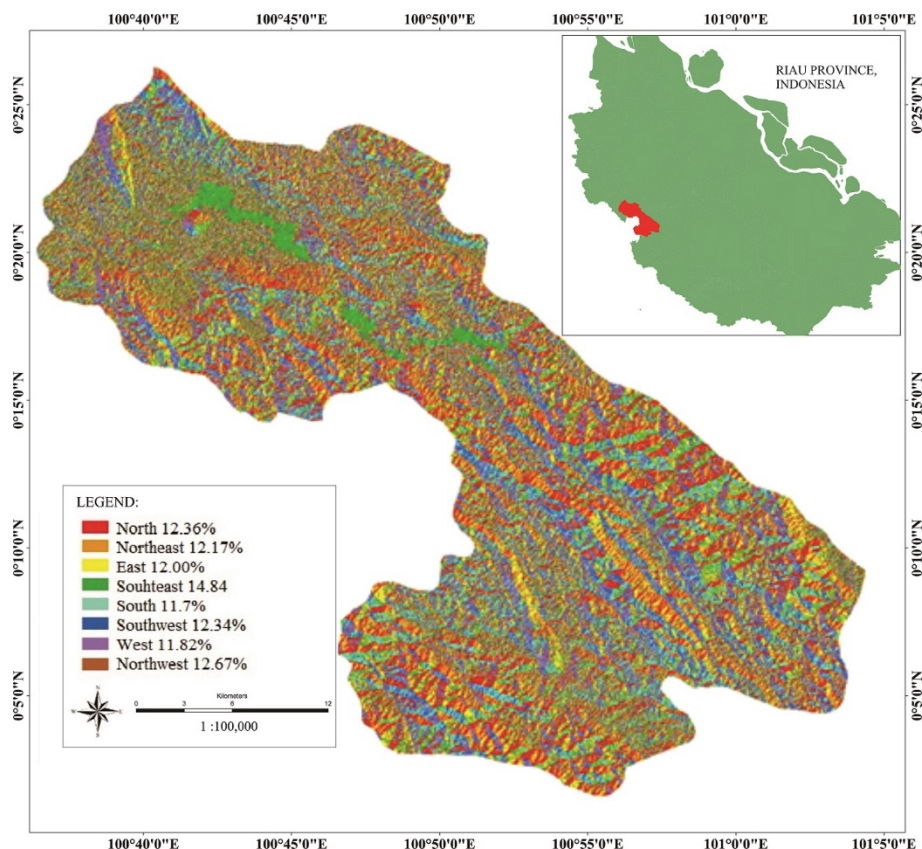


Fig. 18: Straightness of Slope Direction Map of the District of XIII Koto Kampar.

#### 4.8 Rainfall Analysis

The relationship between rainfall and landslides can increase the load on the slopes, causing the slopes to become unstable. Rainfall data in the research area was taken in 2021 from January-December. The average value of rainfall showed that the highest rainfall occurred during the rainy season in July, August, September, October, and November, with a value of respectively 11.981, 13.135, 11.392, 11.596 and 12.340 mm with the peak of rainfall occurring in August, while the highest number of rainy days occurred in November, which was 27 days and the lowest occurred in September with 14 days. Characteristics in the research area as a tropical area are 2276.8 mm of rainfall and 263 spots of rain in one year. The details of average rainfall can be seen in Table 8.

Table 8. Rainfall Analysis in 2021 in the District of XIII Koto Kampar.

No.	Month	Rainfall (mm)	Rain-days	Average Rainfall/month (mm)
1	January	154.1	22	8.561
2	February	108.2	24	4.704
3	March	129.6	25	5.184
4	April	219.4	23	9.539
5	May	168.1	21	8.847

6	June	160.9	21	8.045
7	July	251.6	21	11.981
8	August	223.3	18	13.135
9	September	148.1	14	11.392
10	October	266.7	23	11.596
11	November	308.5	27	12.340
12	December	138.3	24	5.763
Total		2276.8	263	111.088

#### 4.9 Calculation Analysis of Total Landslide Hazard (TEHD) and Landslide Vulnerability Zone Determination (LVZD)

After carrying out all the analysis, the next step is obtaining the calculation of the estimated landslide vulnerability by calculating all the variables that have been used. By analysing the resulting map, then adjusting it to the regional geological map of the research area and adjusting to the digital elevation model data, Landsat-8 OLI imagery, lithology data, slope data, relative relief data, land cover data, land wetness, straightness of slope direction data, and rainfall data for the research area. Furthermore, these data are scored and overlaid on every six maps that have been generated so that four classes of landslide vulnerability are obtained in the research area, which is: very low vulnerability (22.6%), low vulnerability (61.8%), medium vulnerability (15.2%), high vulnerability (0.4%).

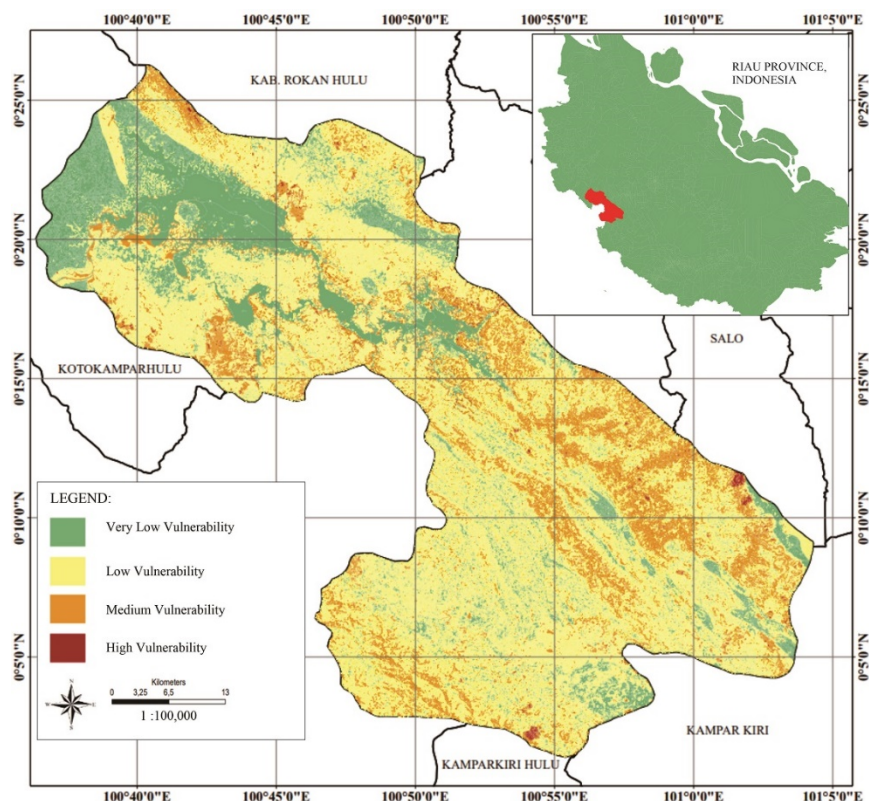


**Fig. 19:** Landslide Vulnerability Map of the District of XIII Koto Kampar.

## 5. Conclusion

This research aims to determine the category of slope failure potential that caused landslides in the research area of XIII Koto Kampar District, Riau Province, Indonesia, as a tropical area with many factors that can cause landslide vulnerability. From the study results, the main factors that influence lithology, slope, relative relief, land cover, the wetness of land, straightness of slope direction to sunlight, and rainfall. These parameters are calculated because the research area is tropical and strongly influenced by changing its natural conditions. The relationship between these factors provides a complete need for calculating the potential for landslides that occur in tropical areas.

## Acknowledgements

The authors would like to thank all who supported this research activity, especially the Government of Kampar District and the Government of Riau Province, for supporting the provision of secondary data. Furthermore, the authors would like to thank Universitas Islam Riau, Chiba University, Japan, and Universitas Merdeka Malang, who continue to support the research collaborations, especially the Geological Engineering Program, Universitas Islam Riau.

## References

- 1) T. Hou, G. Xu, Y. Shen, Z. Wu, N. Zhang, and R. Wang, "Formation mechanism and stability analysis of the houba expansive soil landslide," *Eng. Geol.*, 161 34–43 (2013). doi:10.1016/j.enggeo.2013.04.010.
- 2) R.I. CERRI, F.A.G.V. REIS, M.F. GRAMANI, L.C. GIORDANO, and J.E. ZAINE, "Landslides zonation hazard: relation between geological structures and landslides occurrence in hilly tropical regions of brazil," *An. Acad. Bras. Ciênc.*, 89 (4) 2609–2623 (2017). doi:10.1590/0001-3765201720170224.
- 3) T. Carlà, P. Farina, E. Intrieri, K. Botsialas, and N. Casagli, "On the monitoring and early-warning of brittle slope failures in hard rock masses: examples from an open-pit mine," *Eng. Geol.*, 228 71–81 (2017). doi:10.1016/j.enggeo.2017.08.007.
- 4) H. Sun, X. Wu, D. Wang, H. Xu, X. Liang, and Y. Shang, "Analysis of deformation mechanism of landslide in complex geological conditions," *Bull. Eng. Geol. Environ.*, 78 (6) 4311–4323 (2019). doi:10.1007/s10064-018-1406-3.
- 5) H. Kausarian, E. Trionaldi, T. Khalif Arrahman, D. Bagus eka putra, and Batara, "Settlement and capacity analysis of land support development on flyover in large city; pekanbaru, indonesia," *J. Geosci. Eng. Environ. Technol.*, 5 (2) 103–111 (2020). doi:10.25299/jgeet.2020.5.2.5048.
- 6) J. Peng, X. Tong, S. Wang, and P. Ma, "Three-dimensional geological structures and sliding factors and modes of loess landslides," *Environ. Earth Sci.*, 77 (19) 675 (2018). doi:10.1007/s12665-018-7863-y.
- 7) A. Müller, and E.A. Vargas, "Stability analysis of a slope under impact of a rock block using the

- generalized interpolation material point method (gimp)," *Landslides*, 16 (4) 751–764 (2019). doi:10.1007/s10346-018-01131-1.
- 8) H. Kausarian, A. Suryadi, Susilo, Batara, and J.T.S. Sumantyo, "Flood problem in pekanbaru city analysis using gis approach," *J. Phys. Conf. Ser.*, 1783 (1) 012090 (2021). doi:10.1088/1742-6596/1783/1/012090.
  - 9) K. He, J. Li, B. Li, Z. Zhao, C. Zhao, Y. Gao, and Z. Liu, "The pingdi landslide in shuicheng, guizhou, china: instability process and initiation mechanism," *Bull. Eng. Geol. Environ.*, 81 (4) 131 (2022). doi:10.1007/s10064-022-02596-0.
  - 10) S. Naidu, K.S. Sajinkumar, T. Oommen, V.J. Anuja, R.A. Samuel, and C. Muraleedharan, "Early warning system for shallow landslides using rainfall threshold and slope stability analysis," *Geosci. Front.*, 9 (6) 1871–1882 (2018). doi:10.1016/j.gsf.2017.10.008.
  - 11) A. Quesada-Román, B. Fallas-López, K. Hernández-Espinoza, M. Stoffel, and J.A. Ballesteros-Cánovas, "Relationships between earthquakes, hurricanes, and landslides in costa rica," *Landslides*, 16 (8) 1539–1550 (2019). doi:10.1007/s10346-019-01209-4.
  - 12) H. Kausarian, A. Suryadi, - Susilo, J.T.S. Sumantyo, and - Batara, "GIS analysis for flood problem in the big city: a case study in pekanbaru city, riau province, indonesia," *Int. J. Adv. Sci. Eng. Inf. Technol.*, 11 (1) 342 (2021). doi:10.18517/ijaseit.11.1.11974.
  - 13) R. Anbalagan, "Landslide hazard evaluation and zonation mapping in mountainous terrain," *Eng. Geol.*, 32 (4) 269–277 (1992). doi:10.1016/0013-7952(92)90053-2.
  - 14) D. Kazmi, S. Qasim, I.S.H. Harahap, S. Baharom, M. Imran, and S. Moin, "A study on the contributing factors of major landslides in malaysia," *Civ. Eng. J.*, 2 (12) 669–678 (2016). doi:10.28991/cej-2016-00000066.
  - 15) G. Efremidis, M. Avlonitis, A. Konstantinidis, and E.C. Aifantis, "A statistical study of precursor activity in earthquake-induced landslides," *Comput. Geotech.*, 81 137–142 (2017). doi:10.1016/j.compgeo.2016.08.010.
  - 16) M. Basharat, M.T. Riaz, M.Q. Jan, C. Xu, and S. Riaz, "A review of landslides related to the 2005 kashmir earthquake: implication and future challenges," *Nat. Hazards*, 108 (1) 1–30 (2021). doi:10.1007/s11069-021-04688-8.
  - 17) A.V. Thomas, S. Saha, J.H. Danumah, S. Raveendran, M.K. Prasad, R.S. Ajin, and S.L. Kuriakose, "Landslide susceptibility zonation of idukki district using gis in the aftermath of 2018 kerala floods and landslides: a comparison of ahp and frequency ratio methods," *J. Geovisualization Spat. Anal.*, 5 (2) 21 (2021). doi:10.1007/s41651-021-00090-x.
  - 18) A. Suryadi, F.U. Islami, H. Kausarian, and D.B.E. Putra, "Geophysical survey on open dumping landfill for monitoring spread of leachate: a case study in pekanbaru, riau, indonesia," *J. Geosci. Eng. Environ. Technol.*, 5 (2) 121–126 (2020). doi:10.25299/jgeet.2020.5.2.5340.
  - 19) T.L. Heidrick, and K. Aulia, "A structural and tectonic model of the coastal plains block, central sumatra basin, indonesia," (1993).
  - 20) B. Batara, and C. Xu, "Evolved magmatic arcs of south borneo: insights into cretaceous slab subduction," *Gondwana Res.*, 111 142–164 (2022). doi:10.1016/j.gr.2022.08.001.
  - 21) H. Kausarian, "A new geological map for formation distribution on southern part of south china sea: west kalimantan, indonesia," *Int. J. GEOMATE*, 17 (63) (2019). doi:10.21660/2019.63.ICEE23.
  - 22) R.P. Koesoemadinata, and T. Matasak, "Stratigraphy and sedimentation: ombilin basin, central sumatra (west sumatra province)," (1981).
  - 23) M.C.G. Clarke, W. Kartawa, A. Djunuddin, E. Suganda, and M. Bagdja, "Geological map of the pekanbaru quadrangle, sumatera. harahap bhakti h., syaiful b., baharuddin, suwarna n., panggabea h., simanjuntak to (2003), stratigraphic lexicon of indonesia,(special)," (1982).
  - 24) S. Lee, "Current and future status of gis-based landslide susceptibility mapping: a literature review," *Korean J. Remote Sens.*, 35 (1) 179–193 (2019). doi:10.7780/KJRS.2019.35.1.12.
  - 25) L. Shano, T.K. Raghuvanshi, and M. Meten, "Landslide susceptibility evaluation and hazard zonation techniques – a review," *Geoenvironmental Disasters*, 7 (1) 18 (2020). doi:10.1186/s40677-020-00152-0.
  - 26) T. Xiao, K. Yin, T. Yao, and S. Liu, "Spatial prediction of landslide susceptibility using gis-based statistical and machine learning models in wanzhou county, three gorges reservoir, china," *Acta Geochim.*, 38 (5) 654–669 (2019). doi:10.1007/s11631-019-00341-1.
  - 27) M.Z. Lubis, K. Anggraini, H. Kausarian, and S. Pujiyati, "Review: marine seismic and side-scan sonar investigations for seabed identification with sonar system," *J. Geosci. Eng. Environ. Technol.*, 2 (2) 166 (2017). doi:10.24273/jgeet.2017.2.2.253.
  - 28) M.Z. Lubis, G. Surya, D.S. Pamungkas, B. Subhan, H.M. Manik, H. Kausarian, and W. Anurogo, "Characteristics of waters during transitional season, senimba waters," *Trends Sci.*, 19 (11) 4495 (2022). doi:10.48048/tis.2022.4495.
  - 29) A. Yussupov and Raya Z. Suleimenova, "Use of remote sensing data for environmental monitoring of desertification," *Evergreen*, 10(1) 300–307 (2023). doi:10.5109/6781080.
  - 30) Imas Tri Setyadewi and Purnomo Sidi Priambodo, "Study and analysis of crosstalk reduction in uav cabling by using various cable types," *Evergreen*, 9(1) 150–155 (2022). doi:10.5109/4774232.
  - 31) K.-T. Chang, A. Merghadi, A.P. Yunus, B.T. Pham, and J. Dou, "Evaluating scale effects of topographic

- variables in landslide susceptibility models using gis-based machine learning techniques,” *Sci. Rep.*, 9 (1) 12296 (2019). doi:10.1038/s41598-019-48773-2.
- 32) H. Kausarian, J.T. Sri Sumantyo, D.B. eka Putra, A. Suryadi, and G. Gevisioner, “Image processing of alos palsar satellite data, small unmanned aerial vehicle (uav), and field measurement of land deformation,” *Int. J. Adv. Intell. Inform.*, 4 (2) 132 (2018). doi:10.26555/ijain.v4i2.221.
- 33) A. El Jazouli, A. Barakat, and R. Khellouk, “GIS-multicriteria evaluation using ahp for landslide susceptibility mapping in oum er rbia high basin (morocco),” *Geoenvironmental Disasters*, 6 (1) 3 (2019). doi:10.1186/s40677-019-0119-7.
- 34) E. Psomiadis, A. Papazachariou, K. Soulis, D.-S. Alexiou, and I. Charalampopoulos, “Landslide mapping and susceptibility assessment using geospatial analysis and earth observation data,” *Land*, 9 (5) 133 (2020). doi:10.3390/land9050133.
- 35) H. Kausarian, Lady Redyafry, Josaphat Tetuko Sri Sumantyo, A. Suryadi, and Muhammad Zainuddin Lubis, “Structural analysis of the central sumatra basin using geological mapping and landsat 8 oli/tirs c2 11 data,” *Evergreen*, 10(2) 792–804 (2023). doi:10.5109/6792830.
- 36) Mohammed Ali Berawi, A. Darmawan, Gunawan, P. Miraj, and Hamzah Abdul Rahman, “Land value capture: defining crucial variables difference-in-differences model for residential properties surrounding mrt jakarta stage i,” *Evergreen*, 7(2) 253–261 (2020). doi:10.5109/4055228.
- 37) S. Darmawan, K. Raynaldo, and A. Halim, “Investigation of thruster design to obtain the optimum thrust for rov (remotely operated vehicle) using cfd,” *Evergreen*, 9(1) 115–125 (2022). doi:10.5109/4774224.
- 38) A. Dikshit, R. Sarkar, B. Pradhan, S. Acharya, and A.M. Alamri, “Spatial landslide risk assessment at phuentsholing, bhutan,” *Geosciences*, 10 (4) 131 (2020). doi:10.3390/geosciences10040131.
- 39) Z. Wang, D. Wang, Q. Guo, and D. Wang, “Regional landslide hazard assessment through integrating susceptibility index and rainfall process,” *Nat. Hazards*, 104 (3) 2153–2173 (2020). doi:10.1007/s11069-020-04265-5.
- 40) W. Lin, K. Yin, N. Wang, Y. Xu, Z. Guo, and Y. Li, “Landslide hazard assessment of rainfall-induced landslide based on the cf-sinmap model: a case study from wuling mountain in hunan province, china,” *Nat. Hazards*, 106 (1) 679–700 (2021). doi:10.1007/s11069-020-04483-x.
- 41) Y. Izumi, J. Widodo, H. Kausarian, S. Demirci, A. Takahashi, P. Razi, M. Nasucha, H. Yang, and J. Tetuko S. S., “Potential of soil moisture retrieval for tropical peatlands in indonesia using alos-2 l-band full-polarimetric sar data,” *Int. J. Remote Sens.*, 40 (15) 5938–5956 (2019). doi:10.1080/01431161.2019.1584927.
- 42) M.Z. Lubis, W. Anurogo, H. Kausarian, G. Surya, and T. Choanji, “Sea surface temperature and wind velocity in batam waters its relation to indian ocean dipole (iod),” *J. Geosci. Eng. Environ. Technol.*, 2 (4) 255 (2017). doi:10.24273/jgeet.2017.2.4.778.